J|A|C|S ARTICLES

Published on Web 07/31/2009

Fundamental Reaction Mechanism and Free Energy Profile for (−)-Cocaine Hydrolysis Catalyzed by Cocaine Esterase

Junjun Liu,[†,‡] Adel Hamza,[‡] and Chang-Guo Zhan*[,‡]

Key Laboratory of Pesticide and Chemical Biology of Ministry of Education, College of Chemistry, Central China Normal University, Wuhan 430079, People's Republic of China, and Department of Pharmaceutical Sciences, College of Pharmacy, University of Kentucky, 725 Rose Street, Lexington, Kentucky 40536

Received May 15, 2009; E-mail: zhan@uky.edu

Abstract: The fundamental reaction mechanism of cocaine esterase (CocE)-catalyzed hydrolysis of (−)-cocaine and the corresponding free energy profile have been studied by performing *pseudobond* first-principles quantum mechanical/molecular mechanical free energy (QM/MM-FE) calculations. On the basis of the QM/MM-FE results, the entire hydrolysis reaction consists of four reaction steps, including the nucleophilic attack on the carbonyl carbon of (−)-cocaine benzoyl ester by the hydroxyl group of Ser117, dissociation of (−)-cocaine benzoyl ester, nucleophilic attack on the carbonyl carbon of (−)-cocaine benzoyl ester by water, and finally dissociation between the (−)-cocaine benzoyl group and Ser117 of CocE. The third reaction step involving the nucleophilic attack of a water molecule was found to be rate-determining, which is remarkably different from (−)-cocaine hydrolysis catalyzed by wild-type butyrylcholinesterase (BChE; where the formation of the prereactive BChE−(−)-cocaine complex is rate-determining) or its mutants containing Tyr332Gly or Tyr332Ala mutation (where the first chemical reaction step is rate-determining). Besides, the role of Asp259 in the catalytic triad of CocE does not follow the general concept of the "charge-relay system" for all serine esterases. The free energy barrier calculated for the rate-determining step of CocE-catalyzed hydrolysis of (−)-cocaine is 17.9 kcal/mol, which is in good agreement with the experimentally derived activation free energy of 16.2 kcal/mol. In the present study, where many sodium ions are present, the effects of counterions are found to be significant in determining the free energy barrier. The finding of the significant effects of counterions on the free energy barrier may also be valuable in guiding future mechanistic studies on other charged enzymes.

Introduction

Cocaine is a powerfully addictive stimulant that directly affects the brain and produces a number of toxic effects at high dose. Despite intensive efforts toward education, cocaine abuse continues to be a serious public health problem.[1] Recent surveys in the United States show that cocaine was the first on the list of causes of illicit-drug-related emergency department visits,[2] and cocaine-related emergency department visits increased by 212% between 1995 and 2006, rising from 58 to 181 visits per 100 000 people. The primary toxic effects of cocaine abuse include liver disease, myocardial ischemia, and acute myocardial infarction.[3,4] The sequelae of cocaine overdose include generalized clonic−tonic seizures and status epilepticus capable of producing long-term neurological impairment and death.[5,6] Unfortunately, there is no effective medication for cocaine abuse and toxicity, and the search for effective and safe treatments continues.[7−11]

In chemistry, cocaine can have two enantiomers. One is synthetic and biologically inactive (+)-cocaine, and the other is toxic and naturally occurring (−)-cocaine. Although the classic central nervous system receptor-antagonist approach has failed to yield an anticocaine therapeutic against (−)-cocaine, we have developed a proof of principle for a peripheral blocker to accelerate (−)-cocaine metabolism in the circulation,[12,13] producing biologically inactive metabolites via hydrolysis of

[†] Central China Normal University.
[‡] University of Kentucky.

(1) National Institute on Drug Abuse. *Cocaine Abuse and Addiction*; NIDA Research Report Series; NIH Publication No. 99-4342; National Institutes of Health: Bethesda, MD, 2004 (revd November 2004).
(2) Substance Abuse and Mental Health Services Administration. *Drug Abuse Warning Network, 2004: National Estimates of Drug-Related Emergency Department Visits*; DAWN Series D-28; DHHS Publication No. SMA 06-4143; Office of Applied Studies, Department of Health & Human Services: Rockville, MD, 2006.
(3) Boelsterli, U. A.; Goldlin, C. *Arch. Toxicol.* **1991**, *65* (5), 351–60.
(4) Hahn, I. H.; Hoffman, R. S. *Emerg. Med. Clin. N. Am.* **2001**, *19* (2), 493–510.
(5) Crumb, W. J.; Clarkson, C. W. *Biophys. J.* **1990**, *57* (3), 589–599.
(6) Benowitz, N. L. *Pharmacol. Toxicol.* **1993**, *72* (1), 3–12.
(7) Dickerson, T. J.; Janda, K. D. Recent Advances for the Treatment of Cocaine Abuse: Central Nervous System Immunopharmacotherapy. *Drug Addiction*; Springer: New York, 2008; pp 217−229.
(8) Vocci, F. J.; Acri, J.; Elkashef, A. *Am. J. Psychiatry.* **2005**, *162* (8), 1432–1440.
(9) Pan, Y.; Gao, D.; Yang, W.; Cho, H.; Yang, G.; Tai, H.-H.; Zhan, C.-G. *Proc. Natl. Acad. Sci. U.S.A.* **2005**, *102* (46), 16656–16661.
(10) Gao, D.; Cho, H.; Yang, W.; Pan, Y.; Yang, G.; Tai, H.-H.; Zhan, C.-G. *Angew. Chem., Int. Ed.* **2006**, *45* (4), 653–657.
(11) Zheng, F.; Yang, W.; Ko, M.-C.; Liu, J.; Cho, H.; Gao, D.; Tong, M.; Tai, H.-H.; Woods, J. H.; Zhan, C.-G. *J. Am. Chem. Soc.* **2008**, *130* (36), 12148–12155.
(12) Landry, D. W.; Zhao, K.; Yang, G. X.; Glickman, M.; Georgiadis, T. M. *Science* **1993**, *259* (5103), 1899–1901.

 10.1021/ja903990p CCC: $40.75

(−)-cocaine benzoyl ester.[9,11,14−18] The bacterial cocaine esterase (CocE),[19] which was originally identified in the bacterium *Rhodococcus* sp. strain MB1, is particularly promising. This enzyme is one of the two known enzymes that have evolved under direct selection pressure for (−)-cocaine hydrolysis. It metabolizes (−)-cocaine through hydrolysis of (−)-cocaine benzoyl ester and is the most efficient native cocaine hydrolase yet identified.[20] In rodent models, CocE can both prevent and reverse extreme cocaine toxicity[21,22] and even robustly protects rodents from the lethal effects of cocaine.[23]

A more recent mutagenesis study[24] shows that although native CocE is unstable at physiological temperature, a designed CocE mutant by a novel computational approach aimed at increasing enzyme thermostability yielded a ∼30-fold increase in the plasma half-life both in vitro and in vivo, increasing the probability of clinical application of this enzyme for therapeutic use. The efficiency for CocE as an enzyme therapy for cocaine abuse may also be improved by rational design of CocE mutants aiming at accelerating the rate-determining step of the entire catalytic reaction process while the other steps are not impeded by the mutation. To achieve this end, one must first understand the fundamental mechanisms for CocE-catalyzed hydrolysis of (−)-cocaine. However, the detailed mechanistic issues including the rate-determining step as well as the nature of the transition state have not been addressed.

Recently reported X-ray crystallographic[20] and mutagenesis[25] studies have revealed CocE is a serine carboxylesterase with a catalytic triad formed by Ser117, His287, and Asp259 and with an oxyanion hole formed by the backbone amide of Tyr118 and the hydroxyl group of Tyr44. Mutations on residues in the catalytic triad or oxyanion hole essentially remove catalytic activity against (−)-cocaine. The structural properties of the catalytic triad (Ser117, His287, and Asp259) are very similar to those of the triad in human butyrylcholinesterase (BChE), which consists of Ser198, His438, and Glu325, although the oxyanion hole (Tyr44 and Tyr118) is significantly different from that of BChE, which consists of Gly116, Gly117, and Ala199. It is reasonable to assume (−)-cocaine hydrolysis in CocE undergoes a pathway similar to that in BChE,[15] where the (−)-cocaine hydrolysis consists of two major stages. The first stage is acylation, leading to covalent bond formation between (−)-cocaine and the enzyme and the departure of the ecgonine methyl ester of (−)-cocaine. The second stage is deacylation, resulting in the dissociation of the (−)-cocaine benzoyl ester and enzyme in which a water molecule acts as the nucleophile and the free form of enzyme is restored. On the basis of our initial computational exploration of a possible CocE-catalyzed (−)-cocaine hydrolysis reaction pathway, we propose a hypothesis for the detailed reaction mechanism of (−)-cocaine hydrolysis by CocE (Scheme 1).

Although it is reasonable to assume that (−)-cocaine hydrolysis in CocE undergoes a pathway similar to that in BChE, the proposed mechanism (Scheme 1) may not necessarily be the only choice. The role of the catalytic serine (Ser117) of CocE may not exactly be the same as the role of the catalytic serine (Ser198) of BChE. Alternatively, the Ser117 may act as a general base to activate a water molecule, and the activated water functions as the nucleophile to attack the carbonyl carbon of (−)-cocaine benzoyl ester. According to this alternative mechanistic hypothesis, the entire catalytic hydrolysis reaction consists of only two reaction steps, as depicted in Scheme 2. During the first reaction step, while the water oxygen gradually approaches the carbonyl carbon of (−)-cocaine benzoyl ester, a proton of the water molecule gradually transfers to the hydroxyl oxygen of the Ser117 side chain and the hydroxyl proton of the Ser117 side chain gradually transfers to a nitrogen atom of the His287 side chain. During the second reaction step, the proton which the nitrogen atom of the His287 side chain accepted from the Ser117 side chain gradually transfers to the ester oxygen of the (−)-cocaine benzoyl ester group while the benzoyl ester bond (C−O) is gradually broken.

In the present study, we have examined the feasibility of the two mechanistic hypotheses and, for the feasible mechanistic hypothesis, carried out first-principles quantum mechanical/molecular mechanical free energy (QM/MM-FE) calculations[26−29] to uncover the detailed reaction pathway for the CocE-catalyzed (−)-cocaine hydrolysis reaction. In these QM/MM-FE calculations, first-principles QM/MM reaction coordinate calculations were followed by free energy perturbation (FEP) calculations on the protein environment to account for the dynamic effects of the protein environment on the free energy barriers for an enzymatic reaction. Our QM/MM simulations are based on the pseudobond first-principles QM/MM approach,[26,27,29,30] which has been demonstrated to be a powerful tool in simulating a variety of enzymes,[11,28,31−41] and some theoretical predictions[31,33] were subsequently confirmed by experimental studies.[42−44]

In our current study, the computational results clearly reveal the detailed reaction pathway and the corresponding free energy profile for the CocE-catalyzed (−)-cocaine hydrolysis reaction process. The rate-determining reaction step is thereby identified, and the roles of essential residues including the catalytic triad and oxyanion hole are discussed on the basis of the QM/MM-

(13) Mets, B.; Winger, G.; Cabrera, C.; Seo, S.; Jamdar, S.; Yang, G.; Zhao, K.; Briscoe, R. J.; Almonte, R.; Woods, J. H.; Landry, D. W. *Proc. Natl. Acad. Sci. U.S.A.* **1998**, *95* (17), 10176–10181.
(14) Gorelick, D. A. *Drug Alcohol Depend.* **1997**, *48* (3), 159–165.
(15) Zhan, C.-G.; Zheng, F.; Landry, D. W. *J. Am. Chem. Soc.* **2003**, *125* (9), 2462–2474.
(16) Meijler, M. M.; Kaufmann, G. F.; Qi, L.; Mee, J. M.; Coyle, A. R.; Moss, J. A.; Wirsching, P.; Matsushita, M.; Janda, K. D. *J. Am. Chem. Soc.* **2005**, *127* (8), 2477–2484.
(17) Pan, Y. M.; Gao, D. Q.; Yang, W. C.; Cho, H.; Zhan, C.-G. *J. Am. Chem. Soc.* **2007**, *129* (44), 13537–13543.
(18) Rogers, C. J.; Mee, J. M.; Kaufmann, G. F.; Dickerson, T. J.; Janda, K. D. *J. Am. Chem. Soc.* **2005**, *127* (28), 10016–10017.
(19) Bresler, M. M.; Rosser, S. J.; Basran, A.; Bruce, N. C. *Appl. Environ. Microbiol.* **2000**, *66* (3), 904–908.
(20) Larsen, N. A.; Turner, J. M.; Stevens, J.; Rosser, S. J.; Basran, A.; Lerner, R. A.; Bruce, N. C.; Wilson, I. A. *Nat. Struct. Mol. Biol.* **2002**, *9* (1), 17–21.
(21) Cooper, Z. D.; Narasimhan, D.; Sunahara, R. K.; Mierzejewski, P.; Jutkiewicz, E. M.; Larsen, N. A.; Wilson, I. A.; Landry, D. W.; Woods, J. H. *Mol. Pharmacol.* **2006**, *70* (6), 1885–1891.
(22) Ko, M.-C.; Bowen, L. D.; Narasimhan, D.; Berlin, A. A.; Lukacs, N. W.; Sunahara, R. K.; Cooper, Z. D.; Woods, J. H. *J. Pharmacol. Exp. Ther.* **2007**, *320* (2), 926–933.
(23) Jutkiewicz, E. M.; Baladi, M. G.; Cooper, Z. D.; Narasimhan, D.; Sunahara, R. K.; Woods, J. H. *Ann. Emerg. Med.*, in press.
(24) Gao, D.; Narasimhan, D. L.; Macdonald, J.; Brim, R.; Ko, M.-C.; Landry, D. W.; Woods, J. H.; Sunahara, R. K.; Zhan, C.-G. *Mol. Pharmacol.* **2009**, *75* (2), 318–323.
(25) Turner, J. M.; Larsen, N. A.; Basran, A.; Barbas, C. F.; Bruce, N. C.; Wilson, I. A.; Lerner, R. A. *Biochemistry* **2002**, *41* (41), 12297–12307.
(26) Zhang, Y. *J. Chem. Phys.* **2005**, *122* (2), 024114.
(27) Zhang, Y.; Lee, T.-S.; Yang, W. *J. Chem. Phys.* **1999**, *110* (1), 46–54.
(28) Hu, P.; Zhang, Y. K. *J. Am. Chem. Soc.* **2006**, *128* (4), 1272–1278.
(29) Zhang, Y.; Liu, H.; Yang, W. *J. Chem. Phys.* **2000**, *112* (8), 3483–3492.
(30) Zhang, Y. *Theor. Chem. Acc.* **2006**, *116* (1), 43–50.

Scheme 1. Proposed Catalytic Mechanism for CocE-Catalyzed Hydrolysis of (−)-Cocaine Where Ser117 Acts as a Nucleophile in the First Reaction Step

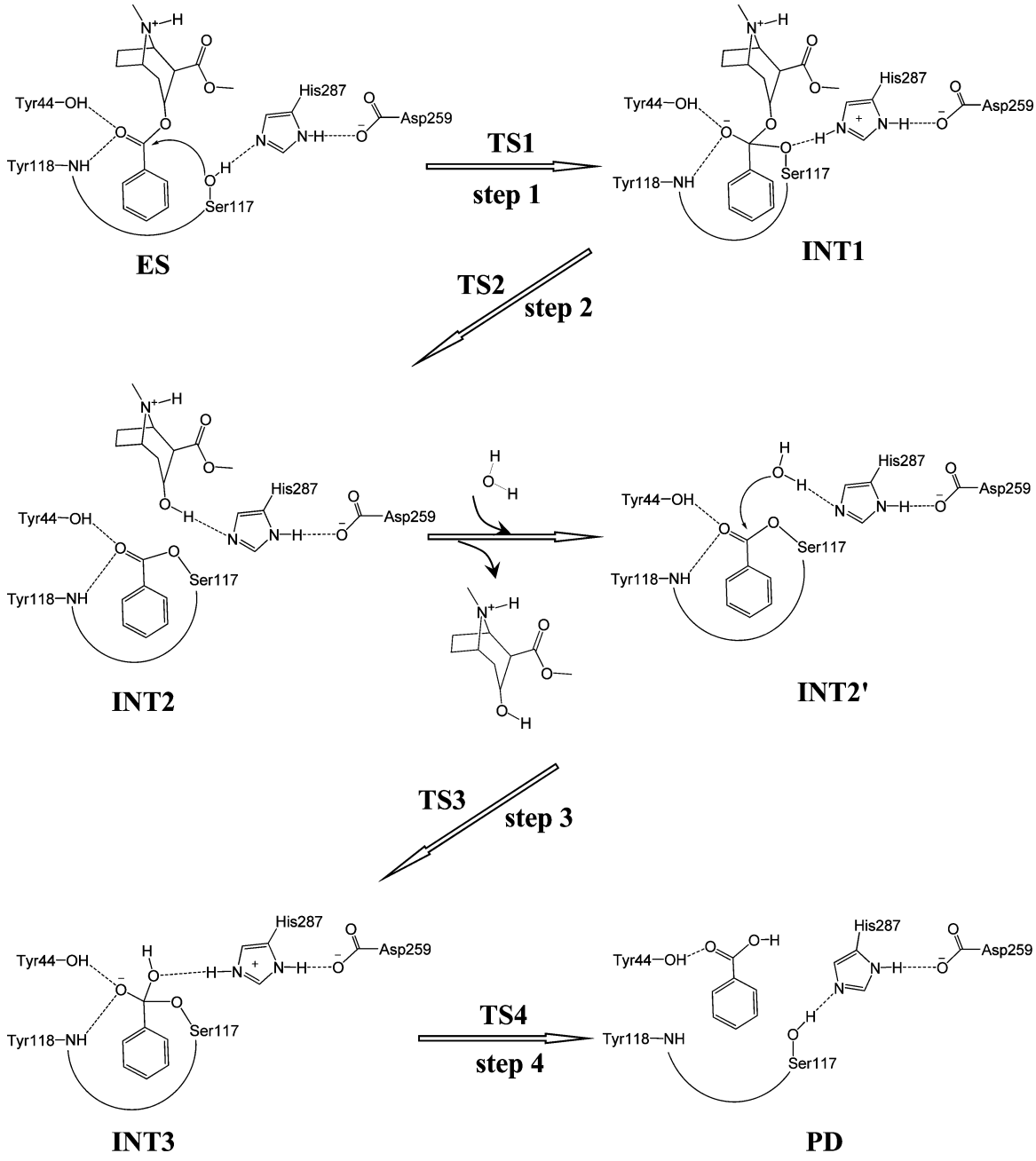

optimized geometries of key configurations in the hydrolysis reaction pathway.

Methods

Structure Preparation. The X-ray crystal structure of CocE (PDB ID 1JU3)[20] and the structure of (−)-cocaine were used in the molecular docking to understand the detailed binding mode of CocE binding with (−)-cocaine. To dock a (−)-cocaine molecule into the active site of the CocE protein, we used a rigid docking method followed by molecular dynamics (MD) simulation. The molecular geometry of (−)-cocaine was optimized by performing ab initio quantum mechanical calculations using the Gaussian03 program[45] at the HF/6-31G* level. The optimized geometry was used to calculate the electrostatic potentials on the molecular surfaces at the same HF/6-31G* level. The calculated electrostatic potentials were used to determine the partial atomic charges by using the standard restrained electrostatic potential (RESP) fitting procedure.[46,47] The determined RESP charges were used for the calculation of electrostatic energies in the docking and MD simulation processes. The missing force field parameters for (−)-cocaine were taken from the general AMBER force field (GAFF) implemented in the AMBER8 program.[48] The molecular docking for each ligand binding was carried out in the same way as we recently did for studying other protein−ligand binding systems.[49,50] We first generated and energy-minimized various molecular orientations and conformations of (−)-cocaine by using the Omega[51] (Open Eye Scientific Software) and AMBER8 programs. Omega sampling is capable of selecting a ligand conformation similar to that of the targeted X-ray crystal structure by using an appropriate option (the default) including a low-energy cutoff to discard high-energy conformations and a low rmsd value below which two conformations are considered to be similar. FRED[52] (Open Eye Scientific Software) docking calculations were carried out using the protein structure with all hydrogen atoms and with

Scheme 2. Possible Catalytic Mechanism for CocE-Catalyzed Hydrolysis of (−)-Cocaine Where Ser117 Acts as a General Base To Activate a Water Molecule and the Activated Water Molecule Acts as a Nucleophile in the First Reaction Step

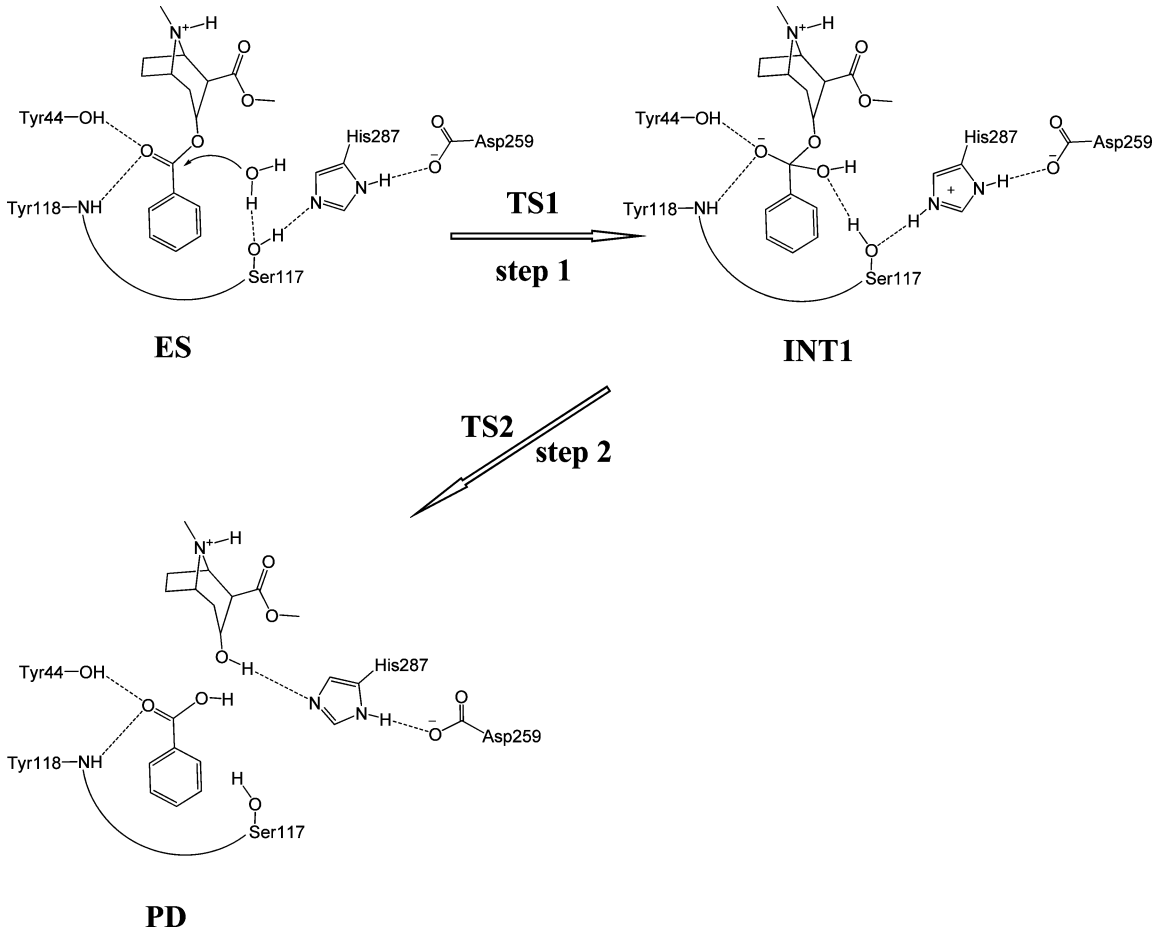

the binding site definition provided by the FRED Receptor program (Open Eye Scientific Software). FRED docking roughly consisted of two steps, i.e., shape fitting and optimization. During the shape fitting, the ligand was placed into a 0.5 Å resolution grid box encompassing all active-site atoms (including hydrogen atoms) using a smooth Gaussian potential. A series of two optimization filters were then processed, consisting of rigid-body optimization and optimization of the ligand pose in the dihedral angle space. As found in the X-ray crystal structure[20] of CocE, the phenyl group of the ligand should first fit between the side chains of the Trp166 and Phe261 residues of the binding site. In separate docking runs, the conformational poses of (−)-cocaine that passed the shape-fitting, optimization filters and interacted with the Trp166 and Phe261 residues were submitted to the MD simulation using the AMBER8 program. During the simulation in a vacuum, the nonbonded cutoff and the dielectric constant were set to group-based (20 Å cutoff distance) and distance-dependent ($\varepsilon = 4r$),[53,54] respectively, to mimic the solvent environment.

Finally, the pose with the lowest interaction energy (sum of the electrostatic and van der Waals interaction energy terms) was selected as the best binding mode and then refined by conducting a ∼3 ns MD simulation in a fully solvated system. It was solvated in a rectangular box of TIP3P water molecules,[55] with a minimum solute wall distance of 10 Å. A total of 33 sodium ions were added to neutralize the charge. As a detailed analysis of the MD-simulated CocE−(−)-cocaine (ES) complex demonstrated that Scheme 2 is not feasible (see below), our QM/MM reaction coordinate calculations were carried out to examine Scheme 1 only. As seen in Scheme 1, there are two reaction stages in the overall CocE-catalyzed hydrolysis of (−)-cocaine. The ecgonine group of (−)-cocaine leaves the system after acylation, resulting in different substrates in the acylation and deacylation stages, i.e., a (−)-cocaine molecule in the acylation stage and a benzoyl group in the deacylation stage. Consequently, we constructed the structure of INT2′ by removing the ecgonine group of (−)-cocaine out of the QM/MM-optimized INT2 structure. The constructed INT2′ was then relaxed by performing a ∼3 ns MD simulation in which the system was also solvated in a rectangular box of TIP3P water molecules[55] with a minimum solute wall distance of 10 Å and was neutralized by adding 34 sodium ions.

For both acylation and deacylation stages, the last snapshots of the MD simulations were used to prepare pseudobond first-principles QM/MM calculations, as the structures in the last snapshots were close to the average structures simulated. Since we are interested in the reaction center, the water molecules beyond 50 Å of the carbonyl carbon atom (C^{ζ}, Figure 1) of the (−)-cocaine benzoyl and all counterions were removed, leaving the QM/MM system with 3469 water molecules and a total of 18 967 atoms for acylation and 3401 water molecules and a total of 18 777 atoms for deacylation. The QM/MM interface has been described by a pseudobond approach.[26,27,30] The boundaries of QM/MM systems for the two stages are defined in Figure 1. Prior to the QM/MM geometry optimizations, each initial reaction system was energy-minimized with the MM method by using the revised AMBER8 program,[48] where the convergence criterion is a root-mean-square deviation (rmsd) of the energy gradient of less than 0.1 kcal·mol^{-1}·Å^{-1}.

(31) Liu, H.; Zhang, Y.; Yang, W. *J. Am. Chem. Soc.* **2000**, *122* (28), 6560–6570.
(32) Zhang, Y.; Kua, J.; McCammon, J. A. *J. Am. Chem. Soc.* **2002**, *124* (35), 10572–10577.

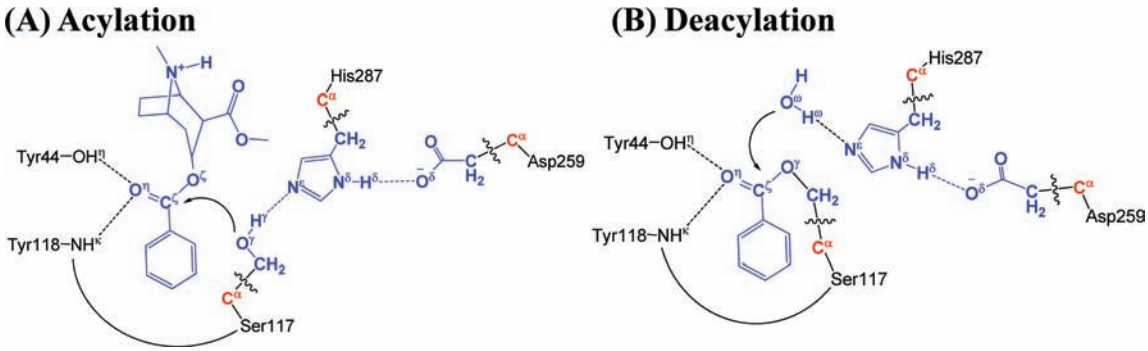

Figure 1. Division of the QM/MM systems for simulating the CocE-catalyzed (−)-cocaine hydrolysis. Atoms in blue are treated by the QM method. Three boundary carbon atoms (C^{α}, colored in red) are treated with the improved pseudobond parameters.[26] All other atoms belong to the MM subsystem.

Minimum-Energy Path of the Enzymatic Reaction. With a reaction coordinate driving method and an iterative energy minimization procedure,[29] the enzyme reaction path was determined by the pseudobond QM/MM calculations at the B3LYP/6-31G*:AMBER level, in which the QM calculations were performed at the B3LYP/6-31G* level of theory by using a modified version of Gaussian03[45] and the MM calculations were performed by using a modified version of the AMBER program.[48] Normal mode analyses were performed to characterize the reactant, intermediates, transition states, and final product. In addition, single-point energy calculations were carried out at the QM/MM(MP2/6-31+G*:AMBER) level on the QM/MM-optimized geometries to evaluate the energy barriers. Throughout the QM/MM calculations, the boundary carbon atoms were treated with improved pseudobond parameters.[26] No cutoff for nonbonded interactions was used in the QM/MM calculations. For the QM subsystem, the convergence criterion for geometry optimizations follows the original Gaussian03 defaults. For the MM subsystem, the geometry optimization convergence criterion is when the rmsd of energy gradient is less than 0.1 kcal·mol^{-1}·Å^{-1}. Prior to QM/MM calculations, the MM subsystem was relaxed by performing ~500 steps of energy minimization with the AMBER8 program. Then atoms within 20 Å of the C^{ζ} atom of the (−)-cocaine benzoyl were allowed to move while all the other atoms outside this range were frozen in all QM/MM calculations, resulting in 2981 movable atoms in QM/MM calculations for acylation and 3089 movable atoms in QM/MM calculations for deacylation.

Free Energy Perturbation. After the minimum-energy path was determined by the QM/MM calculations, the free energy changes associated with the QM−MM interactions were determined by using the FEP method.[29] In FEP calculations, sampling of the MM subsystem was carried out with the QM subsystem frozen at different states along the reaction path. The point charges on the frozen QM atoms used in the FEP calculation are those determined by fitting the electrostatic potential (ESP) in the QM part of the QM/MM calculation. The total free energy difference between the transition state and the reactant was obtained from the following formula:

$$\Delta F(\mathrm{R}\rightarrow\mathrm{TS}) = \Delta F_{\mathrm{qm/mm}}(\mathrm{R}\rightarrow\mathrm{TS}) + \Delta E_{\mathrm{qm}}(\mathrm{R}\rightarrow\mathrm{TS}) + \Delta F_{\mathrm{qm}}^{\mathrm{fluctuation}}(\mathrm{R}\rightarrow\mathrm{TS}) \quad (1)$$

where $\Delta F_{\mathrm{qm/mm}}(\mathrm{R}\rightarrow\mathrm{TS})$ is the free energy change associated with the QM−MM interaction, $\Delta E_{\mathrm{qm}}(\mathrm{R}\rightarrow\mathrm{TS})$ refers to the QM energy difference between the two QM subsystems, and $\Delta F_{\mathrm{qm}}^{\mathrm{fluctuation}}(\mathrm{R}\rightarrow\mathrm{TS})$ is the change in contribution from the QM subsystem fluctuation to the free energy difference.[56] The FEP calculations enabled us to more reasonably determine relative free energy changes due to the QM−MM interaction. Technically, the final (relative) free energy determined by the QM/MM-FE calculations is the QM part of the QM/MM energy (excluding the Coulumbic interaction energy between the point charges of the MM atoms and the ESP charges of the QM atoms) plus the relative free energy change determined by the FEP calculations. In FEP calculations, the time step used was 2 fs, and bond lengths involving hydrogen atoms were constrained. In sampling of the MM subsystem by MD simulations, the temperature was maintained at 298.15 K. Each FEP calculation consisted of 50 ps of equilibration and 300 ps of sampling.

The MD simulations and QM/MM-FE calculations were performed on a supercomputer (e.g., IBM X-series Cluster with 340 nodes or 1360 processors) at the University of Kentucky Center for Computational Sciences. The other modeling and computations

(33) Cisneros, G. A.; Liu, H.; Zhang, Y.; Yang, W. *J. Am. Chem. Soc.* **2003**, *125* (34), 10384–10393.
(34) Zhang, Y.; Kua, J.; McCammon, J. A. *J. Phys. Chem. B* **2003**, *107* (18), 4459–4463.
(35) Cheng, Y.; Zhang, Y.; McCammon, J. A. *J. Am. Chem. Soc.* **2005**, *127* (5), 1553–1562.
(36) Corminboeuf, C.; Hu, P.; Tuckerman, M. E.; Zhang, Y. *J. Am. Chem. Soc.* **2006**, *128* (14), 4530–4531.
(37) Wang, L.; Yu, X.; Hu, P.; Broyde, S.; Zhang, Y. *J. Am. Chem. Soc.* **2007**, *129* (15), 4731–4737.
(38) Wang, S.; Hu, P.; Zhang, Y. *J. Phys. Chem. B* **2007**, *111* (14), 3758–3764.
(39) Xiao, C.; Zhang, Y. *J. Phys. Chem. B* **2007**, *111* (22), 6229–6235.
(40) Hu, P.; Wang, S.; Zhang, Y. *J. Am. Chem. Soc.* **2008**, *130* (12), 3806–3813.
(41) Cheng, Y.; Zhang, Y.; McCammon, J. A. *Protein Sci.* **2006**, *15* (4), 672–683.
(42) Poyner, R. R.; Larsen, T. M.; Wong, S. W.; Reed, G. H. *Arch. Biochem. Biophys.* **2002**, *401* (2), 155–163.
(43) Cisneros, G. A.; Wang, M.; Silinski, P.; Fitzgerald, M. C.; Yang, W. *Biochemistry* **2004**, *43* (22), 6885–6892.
(44) Metanis, N.; Brik, A.; Dawson, P. E.; Keinan, E. *J. Am. Chem. Soc.* **2004**, *126* (40), 12726–12727.
(45) Frisch, M. J.; et al. *Gaussian03*, revision C.02; Gaussian, Inc.: Wallingford, CT, 2004.
(46) Cieplak, P.; Cornell, W. D.; Bayly, C.; Kollman, P. A. *J. Comput. Chem.* **1995**, *16* (11), 1357–1377.
(47) Bayly, C. I.; Cieplak, P.; Cornell, W. D.; Kollman, P. A. *J. Phys. Chem.* **1993**, *97* (40), 10269–10280.
(48) Case, D. A.; et al. *AMBER8*; University of California: San Francisco, 2004.
(49) Bargagna-Mohan, P.; Hamza, A.; Kim, Y. E.; Ho, Y. K. A.; Mor-Valknin, N.; Wendschlag, N.; Li, J. J.; Evans, R. M.; Markovitz, D. M.; Zhan, C.-G.; Kim, K. B.; Mohan, R. *Chem. Biol.* **2007**, *14* (6), 623–634.
(50) Hamza, A.; Zhan, C.-G. *J. Phys. Chem. B* **2009**, *113* (9), 2896–2908.
(51) Bostrom, J.; Greenwood, J. R.; Gottfries, J. *J. Mol. Graphics Modell.* **2003**, *21* (5), 449–462.
(52) McGann, M. R.; Almond, H. R.; Nicholls, A.; Grant, J. A.; Brown, F. K. *Biopolymers* **2003**, *68* (1), 76–90.
(53) Harvey, S. C. *Proteins* **1989**, *5* (1), 78–92.
(54) Guenot, J.; Kollman, P. A. *Protein Sci.* **1992**, *1* (9), 1185–205.
(55) Jorgensen, W. L.; Chandrasekhar, J.; Madura, J. D.; Impey, R. W.; Klein, M. L. *J. Chem. Phys.* **1983**, *79* (2), 926–935.
(56) Zhang, Y.; Liu, H.; Yang, W. In *Methods for Macromolecular Modeling*; Schlick, T., Gan, H. H., Eds.; Springer-Verlag: New York, 2002; pp 332−354.

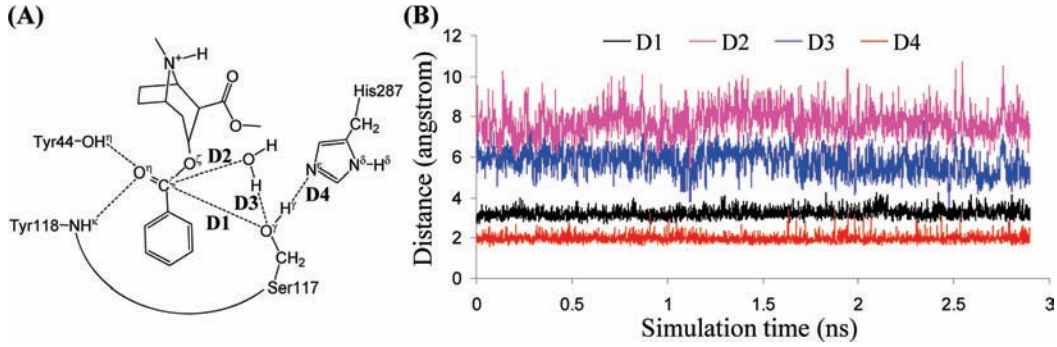

Figure 2. Key internuclear distances (D1 to D4) vs the simulation time in the MD-simulated ES complex.

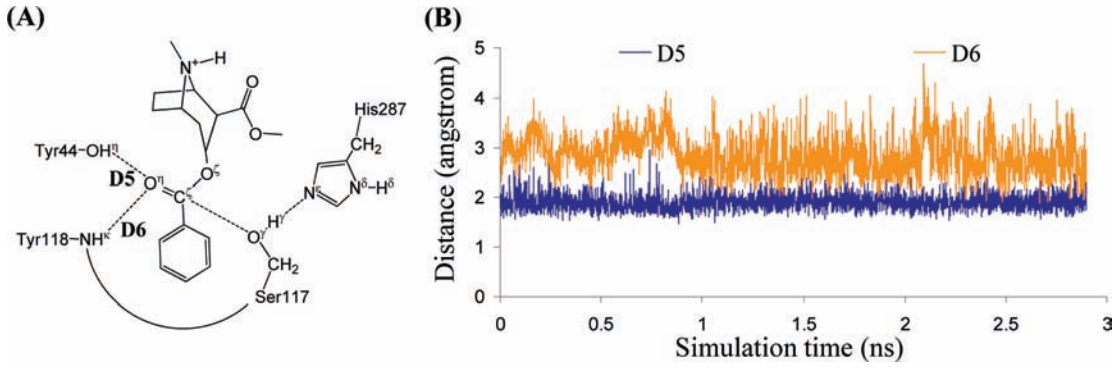

Figure 3. Key internuclear distances (D5 and D6) vs the simulation time in the MD-simulated ES complex.

were carried out on SGI Fuel workstations and a 34-processor IBM x335 Linux Cluster in our own laboratory.

Results and Discussion

Mechanistic Insights from MD Simulations. As shown clearly in Schemes 1 and 2, the key difference between the two mechanistic hypotheses exists in the nucleophile, i.e., Ser117 or the water molecule activated by Ser117. Therefore, it is important for examining the feasibility of the two possible catalytic mechanisms to track the four most crucial internuclear distances, i.e., D1 to D4 depicted in Figure 2, associated with the two possible nucleophiles. Trace D1 is the distance between the carbonyl carbon (C^{ζ}) of (−)-cocaine benzoyl ester and the hydroxyl oxygen (O^{γ}) of the Ser117 side chain. Trace D2 is the distance between the C^{ζ} atom of (−)-cocaine benzoyl ester and the oxygen of the water molecule closest to the C^{ζ} atom for a given snapshot of the MD-simulated structure. We noted that the water molecule closest to the C^{ζ} atom in one snapshot was not necessarily the same as that in another snapshot. Trace D3 in Figure 2 is the distance between the O^{γ} atom of the Ser117 side chain and the water hydrogen atom closest to the O^{γ} atom. Trace D4 is the distance between the hydroxyl hydrogen (H^{γ}) of the Ser117 side chain and the N^{ϵ} atom of the His287 side chain.

As seen in Figure 2B, in the MD-simulated most favorable binding structure of the ES complex, the average value of D2 is ∼7.7 ± 0.7 Å, showing that the water molecules are too far away from the C^{ζ} atom to be the nucleophile. Furthermore, the average value of D3 is ∼5.7 ± 0.6 Å, demonstrating that the interaction between the Ser117 hydroxyl group and the best available water molecule is too weak for Ser117 to activate the water molecule. On the contrary, trace D1 is more stable than D2, and the average value of trace D1 is ∼3.2 ± 0.2 Å, indicating an appropriate distance for the Ser117 hydroxyl performing nucleophilic attack on the C^{ζ} atom. Trace D4 is also more stable than D3, and the average value of D4 is ∼2.0 ± 0.2 Å, showing a strong hydrogen bond between the Ser117 hydroxyl group and the N^{ϵ} atom of the His287 side chain. The MD-simulated ES complex revealed the feasibility of His287 being the general base to activate Ser117 in the nucleophilic attack process. Therefore, it is the hydroxyl group of the Ser117 side chain, rather than a water molecule, that can act as the nucleophile to initiate the hydrolysis reaction.

We also tried to perform the MD simulations using different, less favorable initial ES binding structures obtained from molecular docking. The MD simulations using different initial ES structures also eventually led to a similar ES structure (with similar ranges of the D1, D2, D3, and D4 values) suitable for the mechanism associated with Scheme 1. The MD simulations suggest that the (−)-cocaine hydrolysis in CocE may proceed in a reaction pathway (Scheme 1) similar to that in BChE. The possibility of a reaction pathway associated with Scheme 2 may be excluded in light of the MD simulations.

Fundamental Reaction Pathway. Molecular docking and MD simulation (see Figures 2 and 3) led to a dynamically stable ES complex. Our QM/MM reaction coordinate calculations at the B3LYP/6-31G*:AMBER level starting from the MD-simulated ES complex revealed that the CocE-catalyzed (−)-cocaine hydrolysis reaction consists of four reaction steps. The first reaction step is the nucleophilic attack on the carbonyl carbon (C^{ζ}) of (−)-cocaine benzoyl ester by the O^{γ} atom in Ser117. The second reaction step is the dissociation between (−)-cocaine benzoyl ester and (−)-cocaine ecgonine methyl ester. The third reaction step is the nucleophilic attack on the carbonyl carbon (C^{ζ}) of (−)-cocaine benzoyl ester by a water molecule. The fourth reaction step is the dissociation between the (−)-cocaine benzoyl group and Ser117 of CocE. The optimized geometries of the reactant, intermediates, transition states, and final product are shown in Figures 4−7. Below we discuss each of these reaction steps in detail.

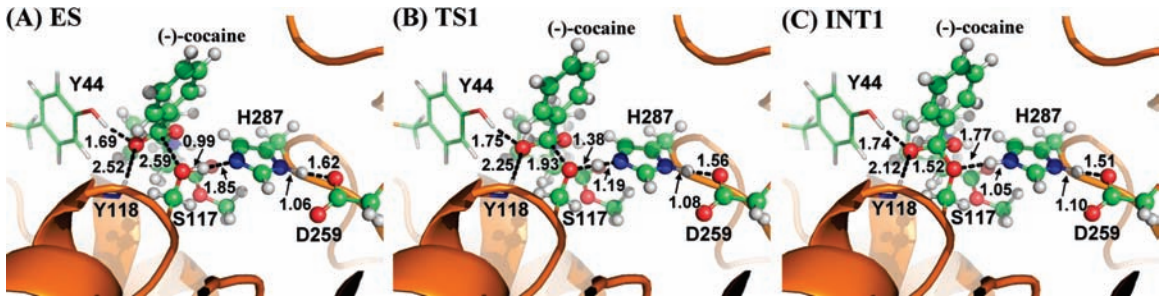

Figure 4. Key configurations for step 1, the nucleophilic attack by the O^{γ} atom of Ser117. The geometries were optimized at the QM/MM(B3LYP/6-31G*:AMBER) level. The key distances in the figure are in angstroms. Carbon, oxygen, nitrogen, and hydrogen atoms are colored in green, red, blue, and white, respectively. The backbone of the protein is rendered as a cartoon and colored in orange. The QM atoms are represented as balls and sticks, and the surrounding residues are rendered as sticks. The figures below are represented using the same method.

Step 1: Nucleophilic Attack on the C^{ζ} Atom by the O^{γ} Atom of Ser117. As shown in Figures 2B and 3B, the binding structure (ES) of the (−)-cocaine molecule in the CocE active site is quite stable. As discussed above, the stable trace D1 suggests (−)-cocaine is at an appropriate distance for nucleophilic attack by Ser117, the nucleophile in the CocE catalytic triad. The strong hydrogen bond between the hydroxyl hydrogen (H^{γ}) of Ser117 and the N^{ε} atom of the His287 side chain indicated by D4 shows that His287, the general base in the CocE catalytic triad, has been positioned and is ready for facilitating the nucleophilic attack process through accepting a proton from the nucleophile. The (−)-cocaine molecule is also stabilized by the oxyanion hole consisting of the backbone amide of Tyr118 and the hydroxyl group of Tyr44. The average values of D5 and D6 shown in Figure 3B are ∼1.9 ± 0.2 and ∼2.8 ± 0.4 Å, respectively, suggesting that two hydrogen bonds are formed between the carbonyl oxygen (O^{η}) of (−)-cocaine and the oxyanion hole. One is a strong hydrogen bond ($O-H^{\eta}\cdots O^{\eta}$) between the Tyr44 hydroxyl and the O^{η} atom of (−)-cocaine, and the other is a weak hydrogen bond ($N-H^{\kappa}\cdots O^{\eta}$) between the Tyr118 NH group and the O^{η} atom of (−)-cocaine. Obviously, Tyr44 plays a more important role in stabilizing the substrate than Tyr118, the other residue in the oxyanion hole, by providing stronger hydrogen bonding.

The nucleophilic attack process then proceeds as the serine hydroxyl oxygen, the O^{γ} atom of Ser117, gradually approaches the C^{ζ} atom of the (−)-cocaine molecule. Meanwhile, the serine hydroxyl hydrogen, the H^{γ} atom of Ser117, gradually moves toward the nitrogen (N^{ε}) atom of the His287 side chain. Since this reaction step involves the breaking of the $O^{\gamma}-H^{\gamma}$ bond and the formation of both $C^{\zeta}-O^{\gamma}$ and $N^{\varepsilon}-H^{\gamma}$ bonds as shown in Scheme 1, the distance between O^{γ} and H^{γ} ($R_{O^{\gamma}-H^{\gamma}}$), the distance between C^{ζ} and O^{γ} ($R_{C^{\zeta}-O^{\gamma}}$), and the distance between N^{ε} and H^{γ} ($R_{N^{\varepsilon}-H^{\gamma}}$) reflect the nature of chemical reaction step 1. Therefore, the reaction coordinate for the current reaction step was set as $R_{O^{\gamma}-H^{\gamma}} - R_{C^{\zeta}-O^{\gamma}} - R_{N^{\varepsilon}-H^{\gamma}}$. As shown in the QM/MM-optimized geometries (Figure 4), as the O^{γ} atom of Ser117 gradually approaches the C^{ζ} atom, the geometry of the reactant (ES) in which the C^{ζ} atom is sp^2-hybridized and is in a planar geometry with its three attached groups gradually changes into a tetrahedral geometry centering on the sp^3-hybridized C^{ζ} atom in an intermediate (INT1) through a transition state (TS1).

Step 2: Dissociation of (−)-Cocaine Benzoyl Ester. In this reaction step, the ecgonine group of (−)-cocaine gradually departs from the (−)-cocaine benzoyl ester group in which the benzoyl ester bond $C^{\zeta}-O^{\zeta}$ is broken. Meanwhile, the proton (H^{γ}) attached to the N^{ε} atom of the His287 side chain transfers to the benzoyl ester oxygen atom (O^{ζ}) of (−)-cocaine. The changes of the distances $R_{C^{\zeta}-O^{\zeta}}$, $R_{O^{\zeta}-H^{\gamma}}$, and $R_{N^{\varepsilon}-H^{\gamma}}$ reflect the nature of a dissociation process. Thus, the reaction coordinate for the current reaction step can be expressed as $R_{C^{\zeta}-O^{\zeta}} + R_{N^{\varepsilon}-H^{\gamma}} - R_{O^{\zeta}-H^{\gamma}}$.

Contrary to what we proposed in Scheme 1 where only one transition state is hypothesized for reaction step 2, the potential energy surface (Figure 5F) which is determined by QM/MM reaction coordinate calculations at the B3LYP/6-31G*:AMBER level shows clearly two transition states in the current reaction process. The two transition states are labeled as TS2 and TS2′. The intermediate between the two transition states is labeled as INT1′. The intermediates and transition states of chemical reaction step 2 were verified by full geometry optimizations followed by harmonic normal mode calculations. The QM/MM-optimized geometries of the intermediates and transition states of the current reaction process are given in Figure 5.

In the geometry of INT1 where the serine hydroxyl proton (H^{γ}) has been transferred to the N^{ε} atom of His287 in reaction step 1, the distance ($R_{O^{\gamma}-H^{\gamma}}$) between the O^{γ} atom of Ser117 and the H^{γ} atom of the His287 side chain is 1.77 Å, indicating a very strong hydrogen bond ($N^{\varepsilon}-H^{\gamma}\cdots O^{\gamma}$) between the Ser117 terminal oxygen and the His287 side chain. However, the distance ($R_{O^{\zeta}-H^{\gamma}}$) between H^{γ} and the leaving ester oxygen (O^{ζ}) to which H^{γ} is about to be transferred is 2.51 Å, indicating a weak hydrogen bond between the H^{γ} atom and the O^{ζ} atom and an unsuitable condition for proton transfer from the N^{ε} atom of His287 to the leaving ester oxygen (O^{ζ}) atom. In changing from INT1 to INT1′, there are two major structural changes. One is the gradual breaking of the covalent bond $C^{\zeta}-O^{\zeta}$ ($R_{C^{\zeta}-O^{\zeta}}$ is 1.60 Å in INT1, 2.04 Å in TS2, and 2.53 Å in INT1′). Another is the formation of a hydrogen bond ($N^{\varepsilon}-H^{\gamma}\cdots O^{\zeta}$) indicated by the shorter and shorter distance $R_{O^{\zeta}-H^{\gamma}}$ in going from INT1 to INT1′ (2.51 Å in INT1, 1.97 Å in TS2, and 1.49 Å in INT1′). In the meantime, the hydrogen bond $N^{\varepsilon}-H^{\gamma}\cdots O^{\gamma}$ formed between the transferring proton (H^{γ}) and the O^{γ} atom of Ser117 becomes progressively weaker ($R_{O^{\gamma}-H^{\gamma}}$ is 1.77 Å in INT1, 1.82 Å in TS2, and 2.38 Å in INT1′), which is reasonable as the transferring proton (H^{γ}) is about to be transferred to the leaving ester oxygen (O^{γ}) in the current reaction step.

The major difference between INT1′ and TS2′ is the position of the transferring proton (H^{γ}) while the distance $R_{C^{\zeta}-O^{\zeta}}$ remains unchanged, indicating that the reaction process associated with TS2′ is primarily the proton (H^{γ}) transfer from the N^{ε} atom of the His287 side chain to the leaving ester oxygen (O^{ζ}) atom ($R_{O^{\zeta}-H^{\gamma}}$ is 1.49 Å in INT1′, 1.30 Å in TS2′, and 1.03 Å in INT2; $R_{N^{\varepsilon}-H^{\gamma}}$ is 1.07 Å in INT1′, 1.17 Å in TS2′, and 1.59 Å in INT2). Normally, the phenyl group of (−)-cocaine benzoyl ester is in the same plane as the sp^2-hybridized carbonyl planar geometry as there is more overlap between the π orbitals, which makes the system more stable. In the geometry of INT2 where (−)-

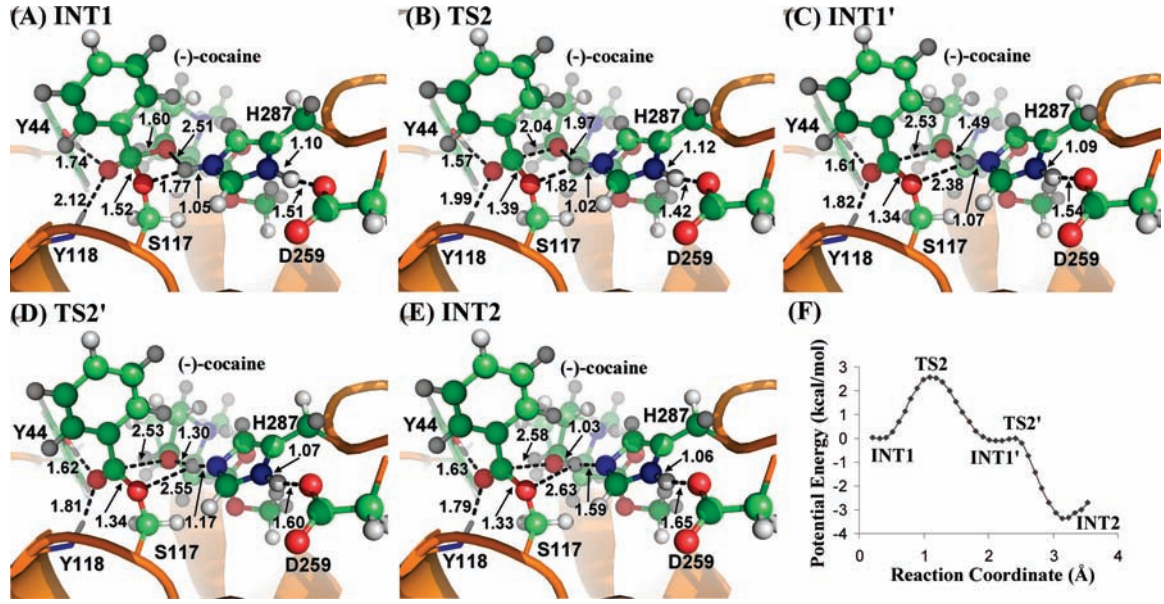

Figure 5. (A−E) Key configurations for step 2, the dissociation of (−)-cocaine benzoyl ester. The geometries were optimized at the QM/MM(B3LYP/6-31G*:AMBER) level. (F) Potential energy of step 2 obtained at the QM/MM(B3LYP/6-31G*:AMBER) level.

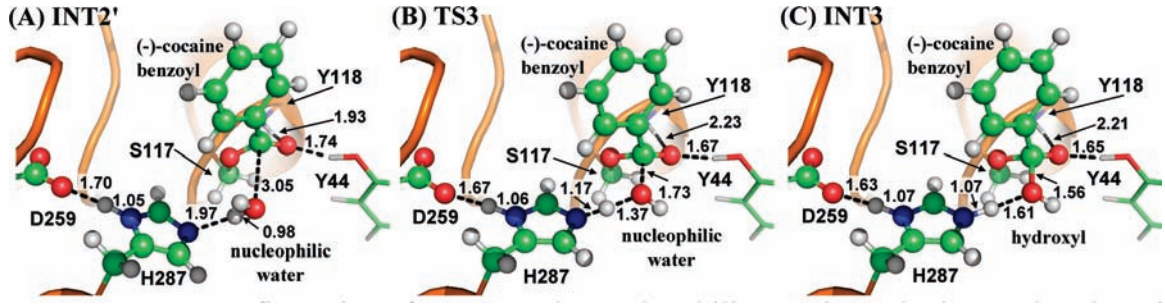

Figure 6. Key configurations for step 3, the nucleophilic attack on the benzoyl carbonyl carbon atom by a water molecule. The geometries were optimized at the QM/MM(B3LYP/6-31G*:AMBER) level.

cocaine has been broken down into ecgonine methyl ester and benzoyl, the benzoyl carbonyl carbon (C^{ζ}) atom becomes sp^2-hybrided again and forms a coplanar shape with the three atoms attached to it. However, the phenyl group in INT2 does not lie in the same plane as the sp^2-hybridized carbonyl. This is probably because the hydrophobic pocket where the (−)-cocaine benzoyl sits is too compact for (−)-cocaine benzoyl to rotate.

According to the two transition states given by the QM/MM potential energy surface, i.e., TS2 and TS2′, the proton transfer proceeds not simultaneously with but only after the breaking of the C−O covalent bond. Technically, there should be one more reaction step in describing the entire hydrolysis reaction, namely, five reaction steps instead of four reaction steps proposed in Scheme 1. However, the calculated energy barrier at the B3LYP/6-31G*:AMBER level for the reaction process associated with TS2′ is only ∼0.1 kcal/mol. Such a small energy barrier is eliminated after the fluctuation of the MM part is accounted for (see below). Therefore, in the present study we still use the notation used in Scheme 1 to describe the hydrolysis reaction pathway. Reaction step 2 involves both $C^{\zeta}-O^{\zeta}$ bond breaking and the proton transfer from the N^{ε} atom to the O^{ζ} atom, and reaction step 3 is still the nucleophilic attack on the C^{ζ} atom by water.

Step 3: Nucleophilic Attack on the C^{ζ} Atom by a Water Molecule. The ecgonine methyl ester was removed from the above-discussed QM/MM-optimized geometry of INT2 to construct the structure of INT2′, which was then relaxed by performing MD simulation. A water molecule close to the carbonyl carbon (C^{ζ}) atom was selected as the nucleophile and was treated by the QM method. The QM/MM-optimized geometry of INT2′ (Figure 6A) at the B3LYP/6-31G*:AMBER level shows that the phenyl group of (−)-cocaine is not completely on the same plane as the sp^2-hybridized carbonyl. The dihedral angle between the plane of the phenyl group and the plane of the sp^2-hybridized carbonyl is 23°. This is probably for the same reason as the not-quite-planar shape of the benzoyl moiety in INT2, which is that the hydrophobic pocket is too compact for the benzoyl to rotate. Similarly to that in the acylation stage, the benzoyl group is also stabilized by the oxyanion hole. As shown in Figure 6A, two strong hydrogen bonds are formed between the carbonyl oxygen (O^{η}) atom of (−)-cocaine and the oxyanion hole in INT2′.

The current nucleophilic process proceeds similarly to reaction step 1, which involves the breaking of the $O^{\omega}-H^{\omega}$ bond and the formation of both $C^{\zeta}-O^{\omega}$ and $N^{\varepsilon}-H^{\omega}$ bonds. Thus, the distances $R_{O^{\omega}-H^{\omega}}$, $R_{C^{\zeta}-O^{\omega}}$, and $R_{N^{\varepsilon}-H^{\omega}}$ were chosen to establish the reaction coordinate as $R_{O^{\omega}-H^{\omega}} - R_{C^{\zeta}-O^{\omega}} - R_{N^{\varepsilon}-H^{\omega}}$ for the current reaction step. In proceeding from INT2′ to INT3 through the transition state TS3 (Figure 6), the coplanar geometry changes into tetrahedral centering on the sp^3-hybridized carbonyl carbon (C^{ζ}) atom as the nucleophilic water gradually approaches the C^{ζ} atom with a spontaneous proton (H^{ω}) transfer from the O^{ω} atom of the nucleophilic water to the N^{ε} atom of the His287 side chain. The QM/MM-optimized geometry of INT3 shows

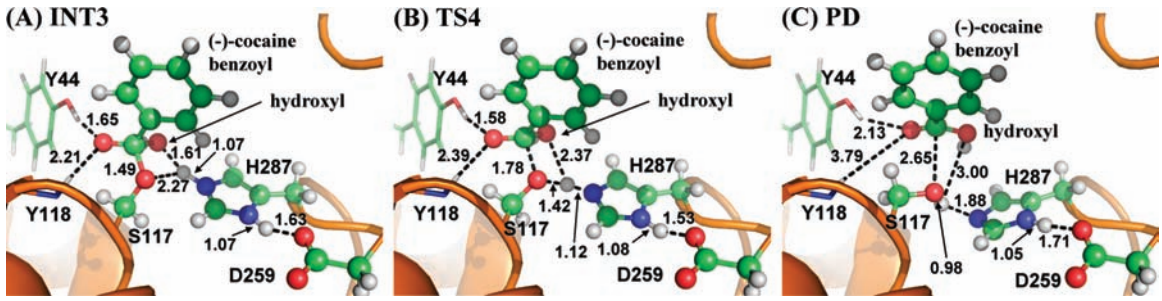

Figure 7. Key configurations for step 4, the dissociation of the (−)-cocaine benzoyl group and Ser117 of CocE. The geometries were optimized at the QM/MM(B3LYP/6-31G*:AMBER) level.

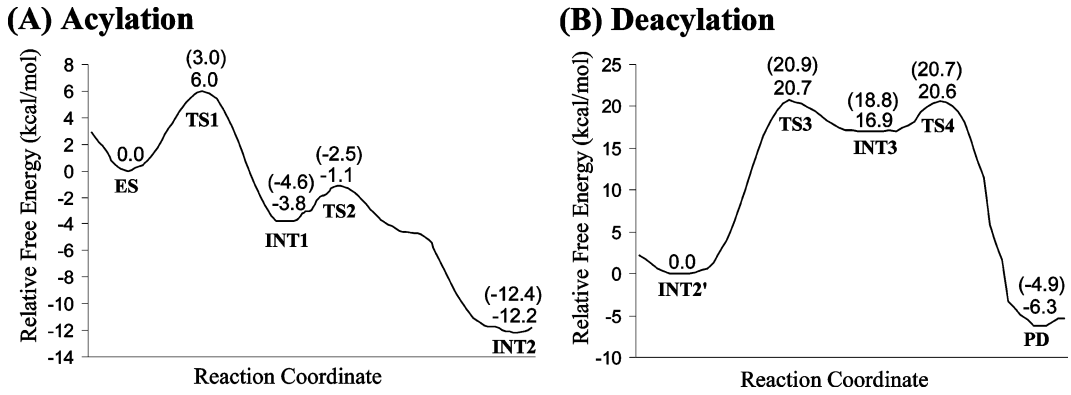

Figure 8. Free energy profile determined by the MP2/6-31+G*:AMBER QM/MM-FE calculations excluding the zero-point and thermal corrections for the QM subsystem. The values in parentheses are relative free energies including zero-point and thermal corrections for the QM subsystem.

that the nucleophilic attack process is completed with water dissociating into hydroxyl attaching to the C^{ζ} atom and a proton (H^{ω}) attaching to the N^{ε} atom.

Step 4: Dissociation between the (−)-Cocaine Benzoyl Group and Ser117 of CocE. The proton transfer between the N^{ε} atom of the His287 side chain and the O^{γ} atom of the Ser117 side chain and the breaking of the covalent bond $C^{\zeta}-O^{\gamma}$ are involved in the dissociation of benzoyl enzyme. The changes of the distances $R_{C^{\zeta}-O^{\gamma}}$, $R_{O^{\gamma}-H^{\omega}}$, and $R_{N^{\varepsilon}-H^{\omega}}$ reflect the nature of reaction step 4. Thus, the reaction coordinate for the current reaction step was expressed as $R_{C^{\zeta}-O^{\gamma}} + R_{N^{\varepsilon}-H^{\omega}} - R_{O^{\gamma}-H^{\omega}}$. Reaction step 4 is similar to reaction step 2, the dissociation of benzoyl ester. In both reaction steps, one type of C−O covalent bond is broken and one proton is transferred from the N^{ε} atom of His287 to the oxygen atom of the broken C−O covalent bond. The difference between the two reaction steps is that the proton transfer in the current reaction step proceeds spontaneously as the C−O bond is gradually broken while that in reaction step 2 does not proceed spontaneously. As shown in Figure 7, in the same time of $C^{\zeta}-O^{\gamma}$ covalent bond breaking, the distance between the O^{γ} atom and H^{ω} atom becomes closer and closer, illustrating a spontaneous proton transfer from the N^{ε} atom of the His287 side chain to the O^{γ} atom of Ser117.

Energetics. Using the QM/MM-optimized geometries at the QM/MM(B3LYP/6-31G*:AMBER) level, we carried out QM/MM single-point energy calculations at the QM/MM(MP2/6-31+G*:AMBER) level for each geometry along the minimum-energy path for both the acylation and deacylation stages of CocE-catalyzed hydrolysis of (−)-cocaine. For each geometry along the minimum-energy path, the ESP charges determined in the QM part of the QM/MM single-point energy calculation were used in subsequent FEP simulations for estimating the free energy changes along the reaction path. Depicted in Figure 8 is the energy profile determined by the QM/MM-FE calculations excluding the zero-point and thermal corrections for the QM subsystem. The values given in parentheses are the corresponding relative free energies with the zero-point and thermal corrections for the QM subsystem.

1. Rate-Determining Step. As shown in Figure 8, the transition state TS2′ of reaction step 2 is eliminated after the free energy changes of the MM part along the reaction path have been applied. The free energy barriers with zero-point and thermal corrections for the QM subsystem of the four reaction steps are 3.0, 2.1, 20.9, and 1.9 kcal/mol, respectively. Obviously, reaction step 3 with a free energy barrier of 20.9 kcal/mol is the rate-determining step of the entire CocE-catalyzed hydrolysis of (−)-cocaine.

It is remarkable to note that the rate-determining step for CocE-catalyzed hydrolysis of (−)-cocaine is different from that for (−)-cocaine hydrolysis catalyzed by BChE. Wild-type BChE has a low catalytic efficiency ($k_{cat} = 4.1$ min^{-1} and $K_M = 4.5$ μM)[57] against (−)-cocaine because residue Tyr332 hinders the formation of the prereactive BChE−(−)-cocaine complex.[58] The combined computational and experimental data and analysis revealed that the rate-determining step of (−)-cocaine hydrolysis catalyzed by BChE mutants containing the Tyr332Gly or Tyr332Ala mutation is the first step of the chemical reaction process.[9] For this reason, the computational design of high-activity mutants of BChE against (−)-cocaine has focused on the stabilization of the transition state for the first reaction step.[9−11,17,58−64] Now that the rate-determining step for CocE-catalyzed hydrolysis of (−)-cocaine is the third reaction step, future computational design of high-activity mutants of CocE

(57) Sun, H.; Pang, Y.-P.; Lockridge, O.; Brimijoin, S. *Mol. Pharmacol.* **2002**, *62* (2), 220–224.
(58) Hamza, A.; Cho, H.; Tai, H.-H.; Zhan, C.-G. *J. Phys. Chem. B* **2005**, *109* (10), 4776–4782.

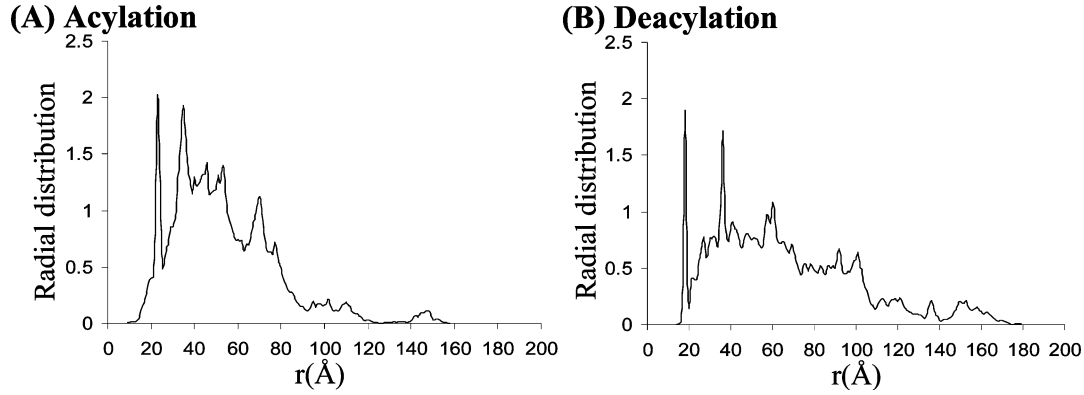

Figure 9. Radial distribution of counterions (Na^+) centered around the C^ζ atom.

against (−)-cocaine should focus on the stabilization of the transition state for the third reaction step.

2. Effects of Counterions. The activation free energy derived from the experimental rate constant ($k_{cat} = 7.8\ s^{-1}$)[20] by using the conventional transition-state theory (CTST)[65,66] is 16.2 kcal/mol. By including zero-point and thermal corrections for the QM subsystem, the free energy barrier of the rate-determining step is ∼20.9 kcal/mol. There is a ∼4.7 kcal/mol difference between the experimental activation free energy and the calculated free energy barrier. This is interesting as the free energy barrier determined by the pesudobond first-principles QM/MM-FE method is usually very close to the experimentally derived activation free energy. The large number of counterions which were not presented in QM/MM calculations draws our attention. There are 33 sodium ions for the acylation stage and 34 sodium ions for the deacylation stage. This large number of counterions should have effects on the QM part, especially in determining energy barriers. A question arises of whether the effects caused by counterions are significant enough to change the hydrolysis pathway revealed by the counterion-excluded QM/MM calculations that is discussed above. To answer this question, a radial distribution of counterions is defined as follows:

$$R(r) = \frac{\sum_{i}^{\text{snapshots}} \frac{N_{j+\delta} - N_j}{r_{j+\delta} - r_j}}{n_{\text{snapshots}}} \qquad (2)$$

where r is the radius with coordinates of the C^ζ atom as the origin, the index i runs over all the snapshots of the equilibrated MD trajectory, the index j runs from 0 to an unlimited number and is increased by a small step size of δ, N_j is the number of counterions within r_j (Å) of the C^ζ atom, and $n_{\text{snapshots}}$ is the number of snapshots. The radial distributions of counterions for both acylation and deacylation stages are depicted in Figure 9. As shown clearly in Figure 9, the counterions are mainly distributed in the range of ∼20 to ∼100 Å to the C^ζ atom that is far from the CocE active site. For both reaction stages, counterions are not found within ∼15 Å of the C^ζ atom, and therefore, we conclude that counterions are not directly involved in the reaction pathway. Therefore, the hydrolysis mechanism described by counterion-excluded QM/MM calculations should not be altered in any way by the effects of counterions.

Since the counterions are so far away from the active site, the van der Waals contribution to the energy barrier of the hydrolysis reaction is negligible. Only the electrostatic contributions from counterions would be important to the energy barrier. Thus, the electrostatic interactions between counterions and the QM subsystem for each key configuration were calculated with the QM method. Such electrostatic interactions of each key configuration could be considered as the approximated correction of counterion effects on the relative energies. To also take into account the fluctuation of counterions, the coordinates of the counterions were taken out every 10 ps from the MD trajectory where the initial structures for QM/MM calculations were taken. A total of 100 snapshots were used for estimating counterion effects. The estimated shift caused by counterion effects on the relative energies for each key configuration are -0.7 ± 0.4, -0.7 ± 0.6, 0.0 ± 0.4, and -0.7 ± 0.8 kcal/mol in the acylation stage from TS1 to INT2, respectively, and -3.0 ± 0.9, -4.0 ± 1.1, -3.2 ± 0.3, and 1.0 ± 1.2 kcal/mol for each key configuration in the deacylation stage from TS3 to PD, respectively. The free energy profile with electrostatic corrections from counterions is replotted in Figure 10. The rate-determining step is still reaction step 3. By including the zero-point and thermal corrections for the QM subsystem, the free energy barrier of the rate-determining step is 17.9 kcal/mol, which is in good agreement with the experimentally derived activation energy of 16.2 kcal/mol.

The effects of counterions could be important in studying the chemical reaction by the QM/MM method. Although counterions may not be directly involved in the reaction mechanism, the interaction between counterions and the QM part is significant in determining the free energy barrier of the reaction when many counterions are present in the system.

Role of the Catalytic Triad and Oxyanion Hole. According to the mechanism described by our pseudobond first-principles QM/MM-FE calculations, the catalytic triad and oxyanion hole are the most essential factors in the CocE-catalyzed hydrolysis of (−)-cocaine. The first residue in the catalytic triad, Ser117, acts as a nucleophile in reaction step 1 and then forms a covalent bond with the carbonyl carbon (C^ζ) atom of (−)-cocaine benzoyl ester until the end of the hydrolysis reaction. The second residue in the catalytic triad, His287, serves as a general base accepting the proton from the nucleophile to facilitate the two nucleophilic

(59) Gao, D. Q.; Zhan, C.-G. *J. Phys. Chem. B* **2005**, *109* (48), 23070–23076.
(60) Zhan, C.-G.; Gao, D. Q. *Biophys. J.* **2005**, *89* (6), 3863−3872.
(61) Gao, D. Q.; Zhan, C.-G. *Proteins* **2006**, *62* (1), 99–110.
(62) Zheng, F.; Zhan, C.-G. *J. Comput.-Aided Mol. Des.* **2008**, *22* (9), 661–671.
(63) Zheng, F.; Zhan, C.-G. *Org. Biomol. Chem.* **2008**, *6* (5), 836–843.
(64) Zhan, C.-G. *Expert Rev. Clin. Pharmacol.* **2009**, *2* (1), 1–4.
(65) Pan, Y. M.; Gao, D. Q.; Zhan, C.-G. *J. Am. Chem. Soc.* **2008**, *130* (15), 5140–5149.
(66) Alvarez-Idaboy, J. R.; Galano, A.; Bravo-Perez, G.; Ruiz, M. E. *J. Am. Chem. Soc.* **2001**, *123* (34), 8387–8395.

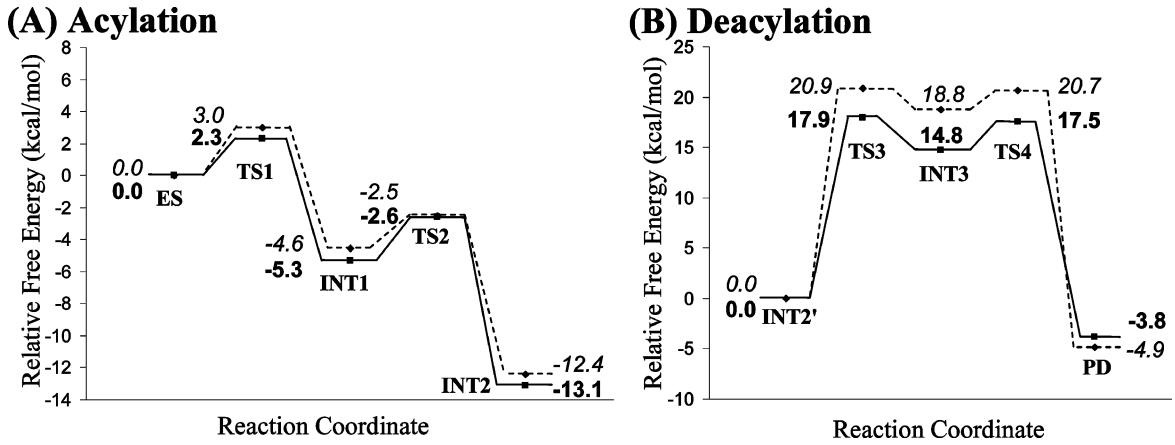

Figure 10. Free energy barriers with (solid line) or without (dashed line) electrostatics corrections from counterions. The energies without electrostatic corrections from counterions are in italics, while those with corrections are in bold. The zero-point and thermal corrections for the QM subsystem are included.

attack processes, i.e., reaction steps 1 and 3. The proton is then donated to the leaving group by His287 in the two dissociation processes, i.e., reaction steps 2 and 4. His287 facilitates either the formation or breaking of the C−O covalent bond in each reaction step. The observations for the two catalytic residues, Ser117 and His287, are basically the same as those of the catalytic triad in other widely studied enzymes. There has been a general concept regarding the role of the third residue in the catalytic triad during the hydrolysis reaction, i.e., Asp259 in CocE. Indeed, the carboxylate of the third residue in the catalytic triad has been suggested as a so-called "charge-relay system" [67,68] to serve as the general-acid−base catalyst, which is involved in the proton transfer between the catalytic aspartic/glutamic acid and the catalytic histidine. It is of particular interest to know whether Asp259 in CocE is involved in a proton transfer between the catalytic histidine and aspartic acid during the CocE-catalyzed hydrolysis of (−)-cocaine concerned in the present study. The answer to this essential mechanistic question can be gleaned from examining two crucial internuclear distances within His287 and Asp259: one ($R_{N^\delta-H^\delta}$) is the distance between the N^δ atom and H^δ atom of the His287 side chain, and the other ($R_{H^\delta-O^\delta}$) is that between the H^δ atom of the His287 side chain and the nearby oxygen (O^δ) of the Asp259 side chain. As seen in Figures 4−7, $R_{N^\delta-H^\delta}$ and $R_{H^\delta-O^\delta}$ are no more than 1.12 Å and no less than 1.42 Å, respectively, among the key configurations along the reaction path, revealing a strong hydrogen bond between His287 and Asp259 but not a proton transfer. As suggested by the relatively shorter distance of the hydrogen bond $N^\delta-H^\delta\cdots O^\delta$ between His287 and Asp259 in the transition states of each reaction step, Asp259 stabilizes the transition states through increasing the strength of its hydrogen bond with His287 during the whole hydrolysis reaction. Such a catalytic role of Asp259 does not follow the general concept of the charge-relay system, but is similar to that of Glu334 in acetylcholinesterase-catalyzed hydrolysis of acetylcholine.[32]

It is also interesting to know the catalytic role of the oxyanion hole consisting of the backbone amide of Tyr118 and the hydroxyl group of Tyr44. On the basis of the QM/MM reaction coordinate calculations, throughout the hydrolysis reaction process, the carbonyl oxygen (O^η) of (−)-cocaine forms two hydrogen bonds with the oxyanion hole. One is the hydrogen bond $O-H^\eta\cdots O^\eta$ with the hydroxyl hydrogen (H^η) atom of the Tyr44 side chain, and the other is the hydrogeon bond $N-H^\kappa\cdots O^\eta$ with the backbone NH group (H^κ atom) of Tyr118. As one can see from Figures 4−7, the hydrogen bond $O-H^\eta\cdots O^\eta$ between the O^η atom and the Tyr44 hydroxyl is very strong throughout the hydrolysis reaction with a distance of ∼1.7 Å. The other hydrogen bond ($N-H^\kappa\cdots O^\eta$) between the O^η atom and Tyr118 backbone NH group is relatively weaker than the one with the Tyr44 hydroxyl during the hydrolysis reaction. It is weak in ES with a distance of ∼2.5 Å and then becomes strong with a distance of ∼2.0 Å in the subsequent states of the hydrolysis reaction. Therefore, both hydrogen bonds stabilize the negative charge of the carbonyl oxygen (O^η) developing during the hydrolysis reaction, where the primary contribution to the stabilization comes from Tyr44. This is also consistent with the mutagenesis study[25] where Tyr44 was mutated to Phe, causing the loss of the hydrogen bond with the carbonyl oxygen (O^η) of (−)-cocaine and resulting in the complete loss of CocE catalytic activity.

Conclusion

The CocE-catalyzed hydrolysis of (−)-cocaine has been studied by using the first-principles QM/MM-FE approach. The detailed reaction pathway has been elucidated. First, a (−)-cocaine molecule binds in the CocE active site with the benzoyl group residing in the hydrophobic pocket. A nucleophilic attack on the carbonyl carbon (C^ζ) of (−)-cocaine benzoyl ester is then carried out by the hydroxyl oxygen (O^γ) of Ser117. This process is facilitated by His287 through proton (H^γ) transfer from the Ser117 hydroxyl to the N^ε atom of the His287 side chain, which increases the nucleophilicity of the Ser117 hydroxyl. His287 is in turn stabilized by another hydrogen bond formation to Asp259. The Ser117 nucleophile attacks the electron-deficient C^ζ atom, forming a tetrahedral intermediate, in which the carbonyl oxygen (O^η) of (−)-cocaine with developing negative charge is stabilized by two tyrosine residues in the oxyanion hole. Then His287 donates a proton (H^γ) to the ester oxygen (O^ζ) of the leaving ecgonine group, completing the acylation stage. Then a water molecule which is activated by His287 initiates the deacylation stage. Reaction processes similar to the acylation stage are repeated in the deacylation stage, and the benzoic acid is released, with CocE being restored to its free form.

(67) Blow, D. M.; Birktoft, J. J.; Hartley, B. S. *Nature* **1969**, *221* (5178), 337–40.
(68) Bachovchin, W. W.; Roberts, J. D. *J. Am. Chem. Soc.* **1978**, *100* (26), 8041–8047.

There are four reaction steps in the hydrolysis reaction. Reaction step 3 where a water molecule attacks the C^{ζ} atom is found to be the rate-determining. Although we did not include the effects of counterions in the QM/MM calculations, the counterions are too far away from the active site and thus do not affect the reaction mechanism as described by our counterion-excluded QM/MM calculations. The calculated free energy barrier with both estimated correction of counterion effects and zero-point and thermal corrections for the QM subsystem is 17.9 kcal/mol, which is in good agreement with the experimentally derived activation free energy of 16.2 kcal/mol. The effects of counterions in the present study, where many sodium ions are present, were found to be significant in determining the free energy barrier. The significant effects of counterions on the free energy barrier found in the present study suggest that one should not ignore the effects of counterions in computational prediction of energy barriers of an enzymatic reaction associated with a charged enzyme.

The role of the catalytic triad and oxyanion hole has also been discussed. The QM/MM-optimized geometries of key configurations of the hydrolysis reaction clearly show no proton transfer between His287 and Asp259, which does not follow the general concept of the charge-relay system. The QM/MM-optimized geometries indicate that the oxyanion hole stabilizes the negative charge of the carbonyl oxygen developing during the hydrolysis reaction by providing two hydrogen bonds from Tyr44 and Tyr118. The hydrogen bond with Tyr44 is particularly strong and is the primary factor in stabilizing the carbonyl oxygen (O^{η}) of (−)-cocaine. This is also consistent with the mutagenesis study where Tyr44 was mutated to Phe, causing the loss of the hydrogen bond with the carbonyl oxygen (O^{η}) of (−)-cocaine and resulting in the complete loss of CocE catalytic activity.

The elucidated reaction mechanism of CocE-catalyzed hydrolysis of (−)-cocaine provides details of the chemical reaction, especially the rate-determining step and the nature of the transition states. The rate-determining step for CocE-catalyzed hydrolysis of (−)-cocaine is remarkably different from that for (−)-cocaine hydrolysis catalyzed by wild-type BChE (where the formation of the prereactive BChE−(−)-cocaine complex is rate-determining) or its mutants containing Tyr332Gly or Tyr332Ala mutation (where the first chemical reaction step is rate-determining). Thus, unlike the computational design of high-activity mutants of BChE against (−)-cocaine, efforts aimed at increasing the catalytic activity of CocE against (−)-cocaine should focus on reaction step 3 where nucleophilic attack on the C^{ζ} atom is carried out by a water molecule.

Acknowledgment. This work was supported in part by the NIH (Grants R01DA013930 and R01DA025100 to C.-G.Z). J.L. worked in C.-G.Z.'s laboratory at the University of Kentucky as an exchange graduate student from Central China Normal University. J.L. thanks A. Goren of Transylvania University (who did sabbatical research in C.-G.Z.'s laboratory) for valuable discussion during the manuscript preparation. We also acknowledge the Center for Computational Sciences (CCS) at the University of Kentucky for supercomputing time on the IBM X-series Cluster with 340 nodes or 1360 processors.

Supporting Information Available: Absolute QM/MM energies (hartrees) calculated at the QM/MM(MP2/6-31+G*:AMBER) level, coordinates of the QM part of the geometries optimized at the QM/MM(B3LYP/6-31G*:AMBER) level, and complete citations of refs 45 and 48. This material is available free of charge via the Internet at http://pubs.acs.org.

JA903990P